CHALMERS
UNIVERSITY OF TECHNOLOGY

Sub-voxel based finite element modelling of fibre-reinforced composites

Software Impacts 21 (2024) 100668

Contents lists available at ScienceDirect

Software Impacts

journal homepage: www.journals.elsevier.com/software-impacts

Original software publication

Sub-voxel based finite element modelling of fibre-reinforced composites

Robert M. Auenhammer [a,*], Carolyn Oddy [a,b], Jisoo Kim [c], Lars P. Mikkelsen [d]

[a] Material and Computational Mechanics, Department of Industrial and Materials Science, Chalmers University of Technology, SE-41296 Göteborg, Sweden
[b] Department of Automation and Composite Technologies, GKN Aerospace Sweden, SE-46138 Trollhättan, Sweden
[c] Strategic Technology Research Institute, Korea Research Institute of Standards and Science, 34113 Daejeon, Republic of Korea
[d] Composites Manufacturing and Testing, Department of Wind and Energy Systems, Technical University of Denmark, DK-4000 Roskilde, Denmark

ARTICLE INFO

Keywords:
Fibre-reinforced composites
Material modelling
Mori–Tanaka
Anisotropic eshelby inclusion
Small-angle X-ray scattering
Tensor tomography

ABSTRACT

For fibre-reinforced composites, most of their mechanical properties is tied to the fibre scale. Thus, imaging-based characterisation demands resolving fibres to characterise these materials accurately. However, high resolutions limit the field of view and lead to lengthy acquisition times. Emerging non-destructive imaging technologies and algorithms now accurately provide fibre orientations without detecting individual fibres. Studies show that voxel sizes up to fifteen times the fibre diameter are feasible, still allowing accurate tensile modulus predictions. Our presented software incorporates sub-voxel fibre orientation distributions using ultra-low-resolution three-dimensional X-ray tomography data in a numerical model, providing an effective method for characterising these materials.

Code metadata

Current code version	*v4.0*
Permanent link to code/repository used for this code version	https://github.com/SoftwareImpacts/SIMPAC-2024-104
Permanent link to Reproducible Capsule	https://codeocean.com/capsule/8442429/tree/v4
Legal Code License	MIT License (MIT)
Code versioning system used	*none*
Software code languages, tools, and services used	*python*
Compilation requirements, operating environments & dependencies	Microsoft Windows, Linux
If available Link to developer documentation/manual	–
Support email for questions	robaue@chalmers.se

1. High-level functionality

Non-destructive three-dimensional X-ray imaging of materials has attracted widespread interest in industrial and research applications. Fibre-reinforced composite materials play a crucial role in various industries, necessitating realistic microstructure modelling for understanding mechanical properties. Existing work on imaging composite materials, using X-ray micro-computed tomography, faces challenges due to the need of resolving individual fibres. High-resolution scans result in large data sets and prolonged acquisition times, imposing limitations on the scanning field of view. Recent progress in image acquisition [1], reconstruction [2] and analysis [3] enables significantly lower image resolutions while retaining sub-voxel microstructure information at a higher speed. This results in a notable decrease in both data size and acquisition/reconstruction/analysis time [4,5]. However, when dealing with voxel sizes three to fifteen times larger than the investigated features (e.g., glass or carbon fibres), novel modelling approaches are required to account for the sub-voxel microstructure. The described software introduces a method, incorporating sub-voxel fibre orientation distributions from orientation tensors for accurate finite element modelling.

Small-angle X-ray scattering tensor tomography offers three-dimensional directional information on microstructures in large volumes, overcoming the limitation by accessing length scales significantly

The code (and data) in this article has been certified as Reproducible by Code Ocean: (https://codeocean.com/). More information on the Reproducibility Badge Initiative is available at https://www.elsevier.com/physical-sciences-and-engineering/computer-science/journals.

* Corresponding author.
E-mail addresses: robaue@chalmers.se (R.M. Auenhammer), carolyn.oddy@chalmers.se (C. Oddy), jisoo.kim@kriss.re.kr (J. Kim), lapm@dtu.dk (L.P. Mikkelsen).

https://doi.org/10.1016/j.simpa.2024.100668
Received 7 May 2024; Accepted 29 May 2024

smaller than a voxel size [6]. With the presented software, we leverage advances in image acquisition to transfer sufficiently accurate local fibre orientations and volume fractions from low-resolution scattering tomography data to a finite element model. Initial results demonstrate significant improvements in the scanning field of interest, surpassing state-of-the-art methodologies for detecting fibre orientations in scans of fibre-reinforced composites by three to six orders of magnitude [7].

The trend towards low-resolution imaging enabled by advances in imaging and image analysis poses challenges for numerical model predicting material properties based on image data. Overcoming this barrier, our software [8] introduces material model construction based on low-resolution imaging data, establishing a new research field denoted as low-resolution image-based modelling. We anticipate significant interest, particularly from industries desiring comprehensive component analyses, making our software timely and impactful.

2. Detailed description of the functionalities

The core of the developed algorithm lies in the refinement of the stiffness matrix based on the sub-voxel fibre orientation distribution. The nominal fibre orientation provided by the scattering tensor for each voxel serves as an approximation of the average fibre orientation within that voxel. However, with a voxel size of 100 µm, roughly fifteen times the diameter of a fibre, multiple fibres contribute to this orientation. This leads to a discrepancy in representing the true mechanical properties due to the nonlinear relationship between stiffness and fibre orientation [7]. Leveraging the information embedded in the scattering tensors, which contain not only the nominal fibre orientation but also details about fibre orientation scattering, enables adjustments of the stiffness matrix at the sub-voxel level. Additionally, the stiffness matrix is constructed based on the sub-voxel fibre volume fraction. The comprehensive process is illustrated in Fig. 1. The individual steps of the algorithm are described in detail in the following:

Ia Load Tensor Tomography data
The tensor tomography data is loaded from four Matlab data files. The fifth order array *'vec.mat'* contains the three eigenvectors of the scattering tensor (3×3 matrix) for each voxel in the three-dimensional grid. The third vector in the fifth dimension of the array represents herein the dominant fibre orientation. The forth order array *'val.mat'* contains the three eigenvalues corresponding to the three eigenvectors of the scattering tensor for each voxel in the three dimensional grid. The fourth order array *'scatt.mat'* contains information about the scattering intensity for each voxel in the three-dimensional grid. From the eigenvalues the mean scattering intensity can be calculated (in [7] see Equation 5). The same applies for the fourth order array *'val_peek.mat'* which stems from the scan of a different sample, which did not contain any fibres but only pure polyetheretherketone (PEEK). The scattering intensity of pure polyetheretherketone (PEEK) is essential to compute a local fibre volume fraction specific to each integration point within the finite element model. This is described in more detail in Step VI.

IIa Create finite element mesh
Hexahedral elements are created at positions in the scanned volume where the scattering intensity is higher than 60% of the mean scattering intensity of the composite. A result of a generated mesh is depicted in Fig. 2. For this mesh, 64 voxels are combined into one element, which contains eight Gauss integration points each. The code further rotates the mesh so that the longitudinal axis of the sample is aligned with the x-axis.

IIIa Compute integration point coordinates
Each hexahedral element contains eight Gauss integration points. For each integration point an individual stiffness matrix is then computed.

Ib Define material properties
The code requires the definition of the following material parameters: mean fibre volume fraction V_{f_mean}, matrix modulus E^m, matrix Poisson's ratio ν^m, longitudinal fibre modulus E_1^f, transverse fibre moduli E_2^f and E_3^f, the fibre shear moduli G_{12}^f, G_{13}^f and G_{23}^f, the fibre Poisson's ratios ν_{12}^f, ν_{13}^f and ν_{23}^f, and the fibre half axes a_1, a_2, a_3.

IIb Compute Eshelby tensor
In the current version of the code the stiffness matrices are computed based on Eshelby's tensor [9] to address the anisotropic nature of carbon fibres and short fibre lengths. Alternative methods for computing the stiffness matrix can be easily integrated. Further details about the computation of Eshelby's tensor and the Mori–Tanaka stiffness matrix [10] can be found in the Supplementary Information of [7].

IIIb Compute stiffness matrix
The Eshelby tensor is applied across the entire sample, under the assumption of consistent fibre dimensions throughout the scanned area. For the mean fibre volume fraction V_{f_mean} and the fibre and matrix material properties a nominal stiffness matrix can be computed.

IV Compute Directional Anisotropy
The novel concept of the Directional Anisotropy (DA) allows to correlate the fibre orientation spread within one voxel to the ratios of the eigenvalues of the scattering tensor (see [7] for more details about the concept and Equations 12 and 13 in [7] for the definition).

V Compute sub-voxel fibre orientation distribution
Based on the values of the Directional Anisotropies (DA) in both xy and xz-plane a spread for the fibre orientation can be calculated. Therefore, the fibre orientation is represented by two fibre orientation angles. These angles are defined as follows: the in-plane angle between the x-axis and the xy-projection of the unit vector, denoted as azimuth (φ), and the angle between the z-axis and the unit vector, denoted as zenith (θ). For each the two angle, ten angles equally distributed around the nominal angles are defined. The degree of spread around the nominal angles increases with higher values of the Directional Anisotropies (see Listing 1).

Listing 1: Computation of the Directional Anisotropy and the fibre orientation angle spread

```
DA_xy = lambda3[g1,g2,g3]/lambda1[g1,g2
    ,g3]
if DA_xy > 0:
    phi_intervall   = DA_xy*np.pi/2
    phi_scat=np.arange(phi_center-
        phi_intervall/2, phi_center+
        phi_intervall/2, phi_intervall
        /10)
else:
    phi_scat=np.array((phi_center,
        phi_center))

DA_xz = lambda3[g1,g2,g3]/lambda2[g1,g2
    ,g3]
if DA_xz > 0:
    theta_intervall = DA_xz*np.pi/2
    theta_scat = np.arange(theta_center
        -theta_intervall/2,
        theta_center+theta_intervall/2,
         theta_intervall/10)
else:
    theta_scat = np.array((theta_center
        , theta_center))
```

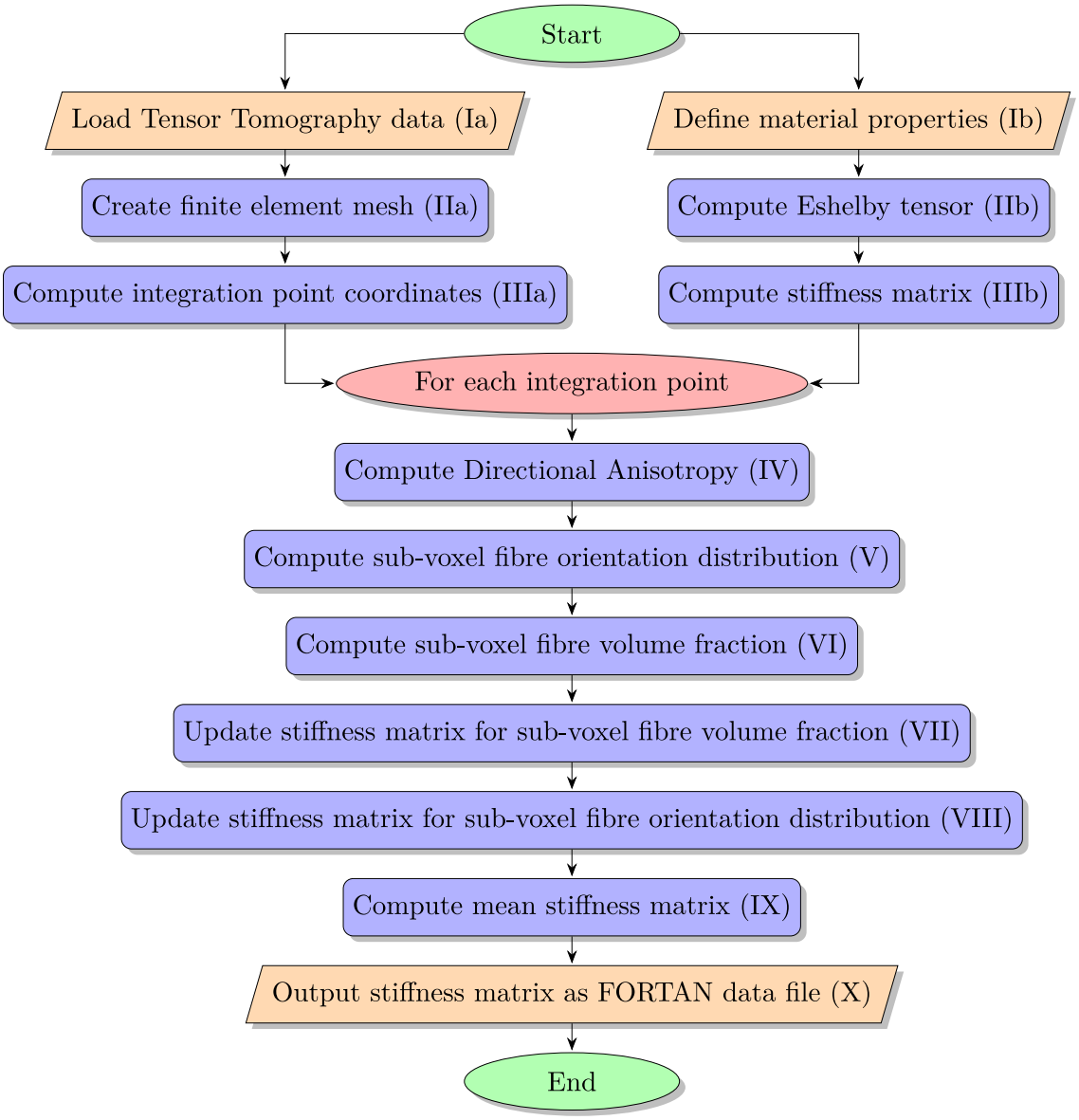

Fig. 1. Flow chart illustrating the algorithm in [8].

VI Compute sub-voxel fibre volume fraction
For each integration point a local fibre sub-voxel fibre volume fraction is calculated. It bases on the principle that a voxel which contains more fibres leads to a higher scattering signal than a voxel with only pure polyetheretherketone (PEEK). Details about the relation can be found in [7] (specifically Equation 16 in [7])

VII Update stiffness matrix for sub-voxel fibre volume fraction
Subsequently, the nominal stiffness matrix, defined in Step IIIb, is updated at each integration point according to the local sub-voxel fibre volume fraction (see Listing 2).

Listing 2: Computation of the local fibre volume fraction of the individual integration point and the update of the stiffness matrix for the respective fibre volume fraction

```
if Vf_tomo[g1,g2,g3]    < 0.1:
    Vf          = 0.1
elif Vf_tomo[g1,g2,g3] > 0.4:
    Vf          = 0.4
else:
    Vf          = Vf_tomo[g1,g2,g3]
C_MT            = computeMT_local(C_m9,
    C_f9, A_MT9, Vf)
C_MT            = np.asarray(C_MT)
C_11            = C_MT[0,0]
C_22            = C_MT[1,1]
C_66            = C_MT[5,5]
C_12            = C_MT[0,1]
C_23            = C_MT[1,2]
```

VIII Update stiffness matrix for sub-voxel fibre orientation distribution
For every of the potential 100 angle combinations per integration point, the stiffness matrix based on the local fibre volume fraction is updated according to the current fibre orientation angles φ and θ (see Listing 3), benefiting from substantial speed enhancements provided by the Python Numba package.

Listing 3: For each combination of φ and θ within the defined angle range new stiffness matrices (36 x 36) are calculated

```
C               = E__update(phi_scat,
    theta_scat, C_11, C_22, C_66, C_12,
     C_23)
```

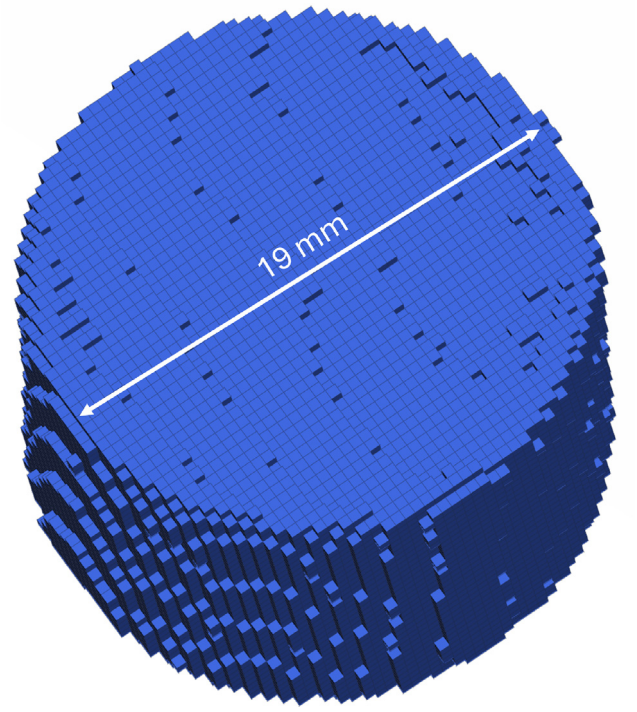

Fig. 2. Automatically generated mesh with hexahedral elements. In this example 64 voxels are combined to one element which contains eight integration points each. In total 65531 elements are depicted.

IX Compute mean stiffness matrix
The process is finalised by computing the mean of all 100 updated stiffness matrices for each individual integration point.

X Output stiffness matrix as FORTAN data file
Finally, the components of the stiffness matrices are output in a FORTRAN data file (Listing 4), readable by the subsequent Abaqus subroutine for the user-defined material model (UMAT), similar to the approach in [11]. Due to symmetry of the stiffness matrix only 30 out of the 36 components are output.

Listing 4: An example of a created FORTRAN data file where for each element the 30 independent stiffness matrix components are stored for each of the eight integration points. In this example the model consists of 8763 elements. Note that not all lines are shown.

```
real*8 E11(8,8763)
real*8 E12(8,8763)
real*8 E13(8,8763)
real*8 E14(8,8763)
real*8 E15(8,8763)
real*8 E16(8,8763)
         .
         .
         .
real*8 E61(8,8763)
real*8 E62(8,8763)
real*8 E63(8,8763)
real*8 E66(8,8763)
integer   :: I
DATA (E11(I,1), I=1,8)/ 8841.0,
    40228.2, 8689.2, 40228.2, &
      40228.2, 40228.2, 8772.3,
          40228.2/
         .
         .
         .
DATA (E66(I,8763), I=1,8)/ 2684.5,
    2684.5, 2684.5, 2684.5, &
      2684.5, 2684.5, 2684.5, 2684.5/
```

3. Impact overview

Demonstrating accurate tensile modulus modelling from low-resolution images (voxel size: 100 µm) of 7 µm diameter carbon fibre-reinforced composites has opened the possibility to increase the scanned volume by three to six orders of magnitude. However, creating an image-based model of this enlarged volumetric size presents novel challenges in image acquisition, data handling, and homogenisation/mapping. While the homogenisation/mapping challenges have been discussed in [12], it is essential to note that the scanned volume remained relatively small in those studies [7,12].

Conventional micro X-ray computed tomography of carbon fibre composites typically necessitates voxel sizes ranging from 1 to 5 µm [13–15]. The data size scales cubed with the voxel size. Opting for a voxel size of 100 µm instead of 1 µm provides a field of view six orders of magnitude larger while keeping the data size constant. Notably, the scanned sample volume ($14 \times 14 \times 19$ mm^3) in [7] surpasses that of other studies, offering insights into the microstructure without the need to individually resolve each fibre.

The utilisation of X-ray small-angle scattering tensor tomography for numerical modelling, as highlighted in previous studies [16,17], is an emerging field, and the proposed software can significantly contribute to the rapid, precise, and automated generation of models from such image data. Furthermore, the software's applicability extends to the commonly used structure tensor method [18–20] in image analysis, which provides a second-order tensor for changes in grey-scale values in conventional micro X-ray computed tomography images. The versatility of our software allows for potential updates, enabling the stiffness matrix to be updated based on the structure tensor instead.

4. Limitations and future improvements/applications

The software is presently tailored for a 100 µm voxel size, set by the X-ray optical element during the initial TOMCAT beamline experiment [7] at the Swiss Light Source. Ongoing efforts focus on refining X-ray optical elements to customise voxel sizes for various micro-structures, potentially necessitating software adjustments. Simultaneously, imaging technology transitions to both a lab-based system and a commercial prototype, expected to produce comparable results [21]. This shift facilitates easier experimental access, meeting a growing demand for subsequent image-based modelling supported by this software.

The presented method of recalculating the stiffness matrix, based on the scattering tensor's shape, relies on an assumed linear correlation between the sub-voxel fibre angle spread and the directional anisotropy derived from the scattering tensor. While the results have proven accurate, alternative correlations, beyond the assumed linear ones, are plausible. A Gaussian weighting has also been tested, assigning higher weights to fibre orientation angles closer to the nominal fibre orientation within the possible fibre angle spread. In the studied case, the difference between a linear correlation and a weighted correlation was negligible. Nevertheless, it is crucial to conduct further investigations to fully comprehend the relationship between sub-voxel fibre angle spread, sub-voxel fibre volume fraction, and directional anisotropy. This understanding is essential for applying the developed approach to various material systems and loading situations.

Despite a successful stiffness matrix update based sub-voxel data for fibre orientation and volume fraction, limitations arise from the large voxel size. While it is feasible to accurately predict tensile modulus and stress distributions, fibrous composites often fail at the fibre level. For instance, carbon fibre-reinforced composites under compression may fail due to a small group of misaligned fibres. Detecting these critical

sub-voxel fibre misalignments requires new strategies. Currently, the software only locally updates the stiffness tensor based on sub-voxel fibre characteristics; however, ongoing exploration aims to include sub-voxel characteristics for material failure criteria. Additionally, a sub-voxel strength update, similar to the stiffness matrix update, can be computed, leading to a recalculation of the ultimate strength (σ^{max} or ϵ^{max}).

List of all scholarly publications enabled by your software:

R. M. Auenhammer, J. Kim, C. Oddy, L. P. Mikkelsen, M. Stampanoni, F. Marone, L. E. Asp. X-ray scattering tensor tomography based finite element modelling of fibre-reinforced composites. npj Computational Materials 10 (2024) 50.

CRediT authorship contribution statement

Robert M. Auenhammer: Investigation, Methodology, Software, Validation, Visualization, Writing – original draft, Writing – review & editing. **Carolyn Oddy:** Investigation, Methodology, Software, Validation, Writing – review & editing. **Jisoo Kim:** Methodology, Software, Writing – review & editing. **Lars P. Mikkelsen:** Funding acquisition, Methodology, Validation, Writing – review & editing.

Declaration of competing interest

The authors declare that they have no known competing financial interests or personal relationships that could have appeared to influence the work reported in this paper.

Declaration of Generative AI and AI-assisted technologies in the writing process

During the preparation of this work the authors used Chat GPT 3.5 in order to improve readability. After using this tool/service, the authors reviewed and edited the content as needed and take full responsibility for the content of the publication.

Acknowledgements

This study was funded by EU Horizon 2020 Marie Skł odowska-Curie Actions Innovative Training Network: MUltiscale, Multimodal and Multidimensional imaging for EngineeRING (MUMMERING), Grant Number 765604. Additional funding was supplied by Fordonsstrategiska Forskning och Innovation, Grant number 2021-05062. This research was also supported by Development of core technologies for advanced measuring instruments funded by Korea Research Institute of Standards and Science (KRISS – 2024 –GP2024-0012).

References

[1] J. Kim, M. Kagias, F. Marone, M. Stampanoni, X-ray scattering tensor tomography with circular gratings, Appl. Phys. Lett. 116 (2020) 134102, http://dx.doi.org/10.1063/1.5145361.

[2] J. Kim, D.M. Pelt, M. Kagias, M. Stampanoni, K.J. Batenburg, F. Marone, Tomographic reconstruction of the small-angle X-Ray scattering tensor with filtered back projection, Phys. Rev. A 18 (1) (2022) 014043, http://dx.doi.org/10.1103/PhysRevApplied.18.014043.

[3] N. Jeppesen, L.P. Mikkelsen, A.B. Dahl, A.N. Christensen, V.A. Dahl, Quantifying effects of manufacturing methods on fiber orientation in unidirectional composites using structure tensor analysis, Composites A 149 (2021) 106541, http://dx.doi.org/10.1016/j.compositesa.2021.106541.

[4] J. Kim, M. Kagias, F. Marone, Z. Shi, M. Stampanoni, Fast acquisition protocol for X-ray scattering tensor tomography, Sci. Rep. 11 (2021) 23046, http://dx.doi.org/10.1038/s41598-021-02467-w.

[5] Y. Sugimoto, D. Shimamoto, Y. Hotta, H. Niino, Estimation of the fiber orientation distribution of carbon fiber–reinforced plastics using small-angle X-ray scattering, Carbon Trends 9 (2022) 100194, http://dx.doi.org/10.1016/j.cartre.2022.100194.

[6] J. Kim, A. Slyamov, E. Lauridsen, M. Birkbak, T. Ramos, F. Marone, J.W. Andreasen, M. Stampanoni, M. Kagias, Macroscopic mapping of microscale fibers in freeform injection molded fiber-reinforced composites using X-ray scattering tensor tomography, Composites B 233 (2022) 109634, http://dx.doi.org/10.1016/j.compositesb.2022.109634.

[7] R.M. Auenhammer, J. Kim, C. Oddy, L.P. Mikkelsen, F. Marone, M. Stampanoni, L.E. Asp, X-ray scattering tensor tomography based finite element modelling of fibre reinforced composites, npj Comput. Mater. 10 (2024) 50, http://dx.doi.org/10.1038/s41524-024-01234-5.

[8] R.M. Auenhammer, C. Oddy, J. Kim, L.P. Mikkelsen, X-ray scattering tensor tomography-based finite element modelling [source code], Code Ocean (2023) http://dx.doi.org/10.24433/CO.6741464.v4.

[9] J.D. Eshelby, The determination of the elastic field of an ellipsoidal inclusion, and related problems, Proc. R. Soc. Lond. A 241 (1957) 376–396.

[10] T. Mori, K. Tanaka, Average stress in matrix and average elastic energy of materials with misfitting inclusions, Acta Metall. 21 (1973) 571–574, http://dx.doi.org/10.1016/0001-6160(73)90064-3.

[11] R.M. Auenhammer, N. Jeppesen, L.P. Mikkelsen, V.A. Dahl, L.E. Asp, X-ray computed tomography data structure tensor orientation mapping for finite element models — STXAE, Softw. Impacts 11 (2022) 100216, http://dx.doi.org/10.1016/j.simpa.2021.100216.

[12] R.M. Auenhammer, A. Prajapati, K. Kalasho, L.P. Mikkelsen, P.J. Withers, L.E. Asp, R. Gutkin, Fibre orientation distribution function mapping for short fibre polymer composite components from low resolution/large volume X-ray computed tomography, Composites B 275 (2024) 111313, http://dx.doi.org/10.1016/j.compositesb.2024.111313.

[13] Y. Wang, Y. Chai, C. Soutis, P.J. Withers, Evolution of kink bands in a notched unidirectional carbon fibre-epoxy composite under four-point bending, Compos. Sci. Technol. 172 (2019) 143–452, http://dx.doi.org/10.1016/j.compscitech.2019.01.014.

[14] D. Wilhelmsson, L.P. Mikkelsen, S. Fæster, L.E. Asp, Influence of in-plane shear on kink-plane orientation in a unidirectional fibre composite, Composites A 119 (2019) 283–290, http://dx.doi.org/10.1016/j.compositesa.2019.01.018.

[15] Y. Sinchuk, O. Shishkina, M. Gueguen, L. Signor, C. Nadot-Martin, H. Trumel, W. Van Paepegem, X-ray CT based multi-layer unit cell modeling of carbon fiber-reinforced textile composites: Segmentation, meshing and elastic property homogenization, Compos. Struct. 298 (2022) 116003, http://dx.doi.org/10.1016/j.compstruct.2022.116003.

[16] R.M. Auenhammer, L.P. Mikkelsen, L.E. Asp, B.J. Blinzler, Automated X-ray computer tomography segmentation method for finite element analysis of non-crimp fabric reinforced composites, Compos. Struct. 256 (2021) 113136, http://dx.doi.org/10.1016/j.compstruct.2020.113136.

[17] R.M. Auenhammer, N. Jeppesen, L.P. Mikkelsen, V.A. Dahl, B.J. Blinzler, L.E. Asp, Robust numerical analysis of fibrous composites from X-ray computed tomography image data enabling low resolutions, Compos. Sci. Technol. 224 (2022) 109458, http://dx.doi.org/10.1016/j.compscitech.2022.109458.

[18] M. Krause, J.M. Hausherr, B. Burgeth, C. Herrmann, W. Krenkel, Determination of the fibre orientation in composites using the structure tensor and local X-ray transform, J. Mater. Sci. 45 (2010) 888–896, http://dx.doi.org/10.1007/s10853-009-4016-4.

[19] I. Straumit, S.V. Lomov, M. Wevers, Quantification of the internal structure and automatic generation of voxel models of textile composites from X-ray computed tomography data, Composites A 69 (2015) 150–158, http://dx.doi.org/10.1016/j.compositesa.2014.11.016.

[20] N. Jeppesen, V.A. Dahl, A.N. Christensen, A.B. Dahl, L.P. Mikkelsen, Characterization of the fiber orientations in non-crimp glass fiber reinforced composites using structure tensor, IOP Conf. Series: Mater. Sci. Eng. 942 (2020) 012037, http://dx.doi.org/10.1088/1757-899x/942/1/012037.

[21] A. Slyamov, J. Kim, M.A. Pedersen, K.K. Nielsen, A.F. Pedersen, T. Ramos, M. Kagias, E. Lauridsen, Towards lab-based X-ray scattering tensor tomography with circular gratings, e-J. Nondestruct. Test. 27 (2022) http://dx.doi.org/10.58286/26573.